ACS APPLIED ELECTRONIC MATERIALS

pubs.acs.org/acsaelm Article

Dynamics of the Bulk-to-Topological State Scattering of Photoexcited Carriers in Bi_2Se_3 Thin Films

Valerio Campanari, Daniele Catone, Patrick O'Keeffe, Alessandra Paladini, Stefano Turchini, Faustino Martelli,* Matteo Salvato, Nouha Loudhaief, Elena Campagna, and Paola Castrucci

Cite This: https://doi.org/10.1021/acsaelm.3c00787 Read Online

ACCESS | Metrics & More | Article Recommendations | Supporting Information

ABSTRACT: Carrier dynamics in polycrystalline Bi_2Se_3 topological insulator thin films were investigated by femtosecond transient absorption spectroscopy (FTAS) at 77 K, by using an infrared pump photon of 0.62 eV energy and a white supercontinuum probe ranging from the near infrared to ultraviolet regions (0.9−3.5 eV). The Bi_2Se_3 samples were grown by vapor solid deposition, a quick, inexpensive, and easy-to-control growth technique to obtain films of different thicknesses, endowed with topological properties. FTAS spectra present several absorption bleaching signals, which can be attributed to electronic transitions involving both bulk and surface states present in the complex Bi_2Se_3 band structure. We observe clear differences in the rise times of several bleaching signals, differences that can be attributed to different band filling dynamics. Fast rise times are observed for transitions only involving bulk states, while a delayed onset of the bleaching signal has been observed for transitions involving surface topological states, which are more efficiently populated by carrier−phonon scattering of bulk electrons and holes, rather than by direct photoexcitation. The observed features shed fresh insights into the properties that allow these materials to be employed as innovative, low-cost, and wide-range photodetectors.

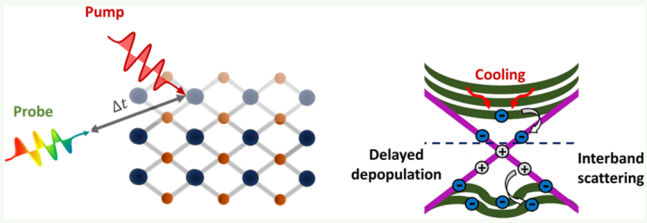

KEYWORDS: *Bi_2Se_3, topological insulators, carrier dynamics, transient absorption spectroscopy*

■ INTRODUCTION

Topological insulators (TIs) have emerged as a new state of matter where the two-dimensional (2D) surface[1] electrons are characterized by Dirac dispersion and spin-momentum locking.[2] The spin-momentum locking and the presence of a bulk bandgap offer new opportunities in fields such as spintronics, superconducting quantum computing,[3] and optoelectronics.[4] From this perspective, Bi_2Se_3, with its high surface mobility[5] $\mu = 10^3–10^4$ cm^2 V^{-1} s^{-1} and relatively large bulk energy bandgap $E_G = 0.32$ eV,[6] is the most promising among the TIs to explore broadband photodetection ranging from ultraviolet (UV) to infrared (IR)[7] and THz.[8]

The crystal structure of Bi_2Se_3 is rhombohedral with a unit cell containing three blocks piled up along the [001] direction, each formed by five atomic layers in the sequence Se−Bi−Se−Bi−Se.[9] The layers inside each block are strongly ionically bonded, while the different blocks (called a quintuple layer, QL) are weakly held together by van der Waals forces. This property allows Bi_2Se_3 thin films to be grown on almost any kind of substrate, independently of the lattice mismatch.[10,11] The possibility of obtaining a wideband optical absorber with a metallic surface, together with the ease of integration with other semiconducting materials, motivates the recent use of Bi_2Se_3 as a component for optoelectronic nanodevices. A new fabrication method based on vapor solid deposition (VSD) on n-doped silicon or glass substrates provides stoichiometric Bi_2Se_3 ultrathin films[12] that grow well-oriented along the [001] crystallographic direction, even on glass. This feature makes them similar to the samples cleaved from bulk materials in ultrahigh vacuum (UHV). In particular, samples grown on n-doped silicon substrates show a bulk insulating nature (i.e., the Fermi level (E_F) lies within the bandgap). In contrast, a frequent limitation of other techniques, such as molecular beam epitaxy (MBE),[11] pulsed laser deposition,[13] chemical vapor deposition,[14] or different methods of VSD,[15] is that they produce n-type Bi_2Se_3 films due to Se vacancies. In this case, the E_F lies within the conduction band, giving rise to a conducting bulk that obscures the topological properties of the film.[12]

In general, for Bi_2Se_3 films above ∼6 QL (about 6 nm), the material takes the form of a gapless 3D TI phase, i.e., with the presence of a Dirac cone within the bulk bandgap and a second Dirac cone at higher energy. The band structure of the gapless 3D TI phase of Bi_2Se_3[16−21] is qualitatively and partially sketched in Figure 1a. It is important to highlight the presence

Received: June 13, 2023
Accepted: July 9, 2023

Downloaded via 141.108.253.146 on July 21, 2023 at 15:47:25 (UTC).
See https://pubs.acs.org/sharingguidelines for options on how to legitimately share published articles.

ACS Publications © XXXX The Authors. Published by American Chemical Society

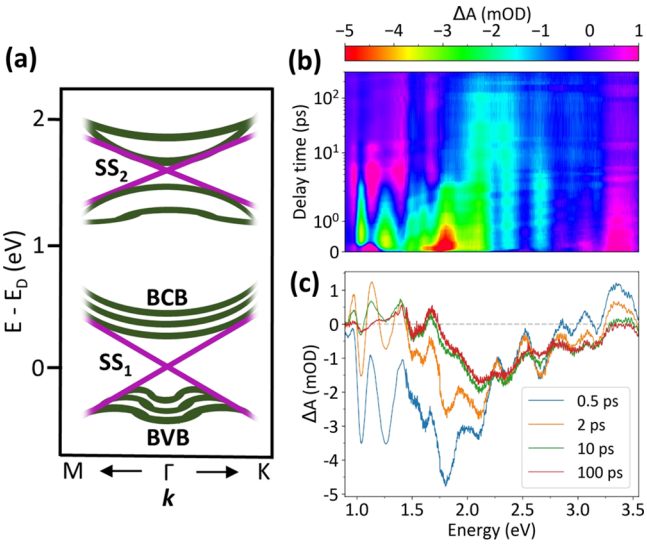

Figure 1. (a) Schematic representation of the band structure of Bi_2Se_3 following that proposed by Sobota et al.:[30] bulk valence band (BVB), bulk conduction band (BCB), first surface Dirac cone (SS_1), second surface Dirac cone (SS_2), and some other bulk energy levels are depicted in the figure. E_D is the Dirac point energy. The figure has an illustrative and qualitative purpose and should not be considered an accurate and quantitative description of Bi_2Se_3 band structure. (b,c) Near-IR to UV femtosecond transient absorption spectra of the Bi_2Se_3 film. (b) False-color map of the transient spectra with the delay time axis in the logarithmic scale. (c) Transient spectra taken at different delay times.

of a first group of bands around the E_F: the bulk valence band (BVB), the bulk conduction band (BCB), separated by a ∼ 0.3 eV bandgap, and the first Dirac cone (SS_1). Moreover, a second group of bulk bands with a second Dirac cone (SS_2) is placed ∼1.7 eV above SS_1.

The material response to optical excitation and the subsequent carrier dynamics are of primary importance for device applications of Bi_2Se_3 thin films. Ultrafast spectroscopy gives important information on the carrier dynamics, and femtosecond transient absorption spectroscopy (FTAS) has been successfully employed on Bi_2Se_3, mainly in the form of epitaxial films grown by MBE.[22−27]

The aim of the present work is to use FTAS to characterize an ∼8 nm Bi_2Se_3 polycrystalline film grown on a glass substrate, to unravel the electronic properties and to show how ultrafast techniques give useful information on the possible employment and optimization of these films in efficient devices. Our measurements were performed at 77 K on films grown by a recently developed VSD method,[12] with a low-energy pump, E_p of ∼0.62 eV (2000 nm), and a very broad UV−vis−IR probe (from 3.5 down to 0.9 eV). The results allow us to reveal the presence of surface topological states and the mechanisms that underlie the carrier scattering between bulk and topological states and to demonstrate the insulating nature of the bulk material, thus showing how the new growth method provides a device suitable material even on an amorphous substrate like glass. Further measurements taken with a different pump energy (1.5 eV, 830 nm) and on samples of different thicknesses (t = 3 nm) confirm the picture obtained for an E_p of ∼0.62 eV and t = 8 nm, the parameters that we will mainly describe in the text. Our measurements are compared, when possible, to the previous measurements made on Bi_2Se_3 grown by MBE and give a more robust picture of the carrier dynamics in gapless 3D TI Bi_2Se_3.

■ EXPERIMENTAL SECTION

FTAS Experimental Setup. The pump−probe experiments were performed using a laser system consisting of a 1 kHz, 4 mJ, 35 fs chirped pulse amplifier seeded by a Ti:Sa oscillator, and the pump pulse was generated by an optical parametric amplifier (OPA). The experimental results reported in this work were obtained with pump wavelengths of 2000 and 830 nm. The probe for the visible region (350−750 nm) was generated by focusing a small quantity of 800 nm light into a rotating CaF_2 crystal and then collimating the white light supercontinuum thus generated. The probe for the IR region above 900 nm (900−1400 nm) was generated in a similar manner by focusing a small quantity of 800 nm light (1−3 μJ) into a YAG crystal. On the other hand, the probe for the IR region between 750 and 900 nm was generated with the same method but starting from a 1300 nm laser pulse, obtained from an in-house developed OPA. The optical layout of the commercial transient absorption spectrometer (Femto-Frame II, IB Photonics) consisted of a split beam configuration for the UV and visible regions in which 50% of the white light passed through the sample while the remainder was used as a reference to account for pulse-to-pulse fluctuations in white light generation. For the IR probe region, a single detector was used with all probe light passing through the sample. The pump pulse was focused (circular spot diameter = 200 μm) onto the sample with a power density of 1.1 mJ/cm^2. The probe spot was much smaller (approximately 150 μm), and its pulse was delayed with respect to the pump by varying the length of its optical path.[28,29]

Sample Preparation. Bi_2Se_3 thin films were obtained by a two-step vapor solid deposition (VSD) method[12] using a Carbolite TF1-1600 furnace. In the first step, the Bi_2Se_3 powder (Sigma Aldrich, granular, ≥99.995% trace metal basis) was evaporated at the temperature of 580 °C in a quartz tube under Ar at a pressure of 5 mbar for 1 h. During cooling, the material was deposited on the inner walls of the quartz tube under an Ar flow rate of 50 sccm. This caused a partial loss of Se, which is more volatile than Bi, and it was pumped by the pumping system. At the end of the first step, the quartz tube was opened, and it was loaded with the substrates and a given quantity of Se, enough to make up for the loss suffered during the first step. During the second step, the Se and the species attached to the tube wall evaporated at the temperature of 600 °C under the pump streaming toward the substrates that are positioned in the coldest part of the tube. Bi_2Se_3 films with different thicknesses were obtained depending on the position of the substrates along the quartz tube, and, thanks to the added Se quantity, they showed the correct stoichiometry. Due to their van der Waals nature, the Bi_2Se_3 films grow with the [001] crystallographic direction perpendicular to the substrate surface.[12] The NIR−vis−UV steady-state absorption spectra of the samples are reported in Figure S1, in the Supporting Information (SI).

■ RESULTS AND DISCUSSION

Results. Figure 1 shows the FTAS spectra in a 2D false-color map (Figure 1b) and transient spectra at representative delay times (Figure 1c). The measurements show a feature-rich spectrum with multiple, overlapping photoinduced absorption bleaching (PB) signals, which form a broad feature over the whole probe range. From this broad signal, some resolvable PBs (negative minima) emerge at 1.03, 1.13, 1.50, 1.60, 1.80, 2.10, 2.35, 2.66, 2.95, and 3.17 eV. Moreover, some positive signals are observed, especially below 1.40 eV and above 3.20 eV, but their low intensity makes them more difficult to be better identified. In Figure S2, we compare results of the samples with 8 and 3 nm thickness. The transient absorption spectra of the two samples are reported for the probe delay time of 1 ps. The similarity of the spectra is evident, the main

https://doi.org/10.1021/acsaelm.3c00787
ACS Appl. Electron. Mater. XXXX, XXX, XXX−XXX

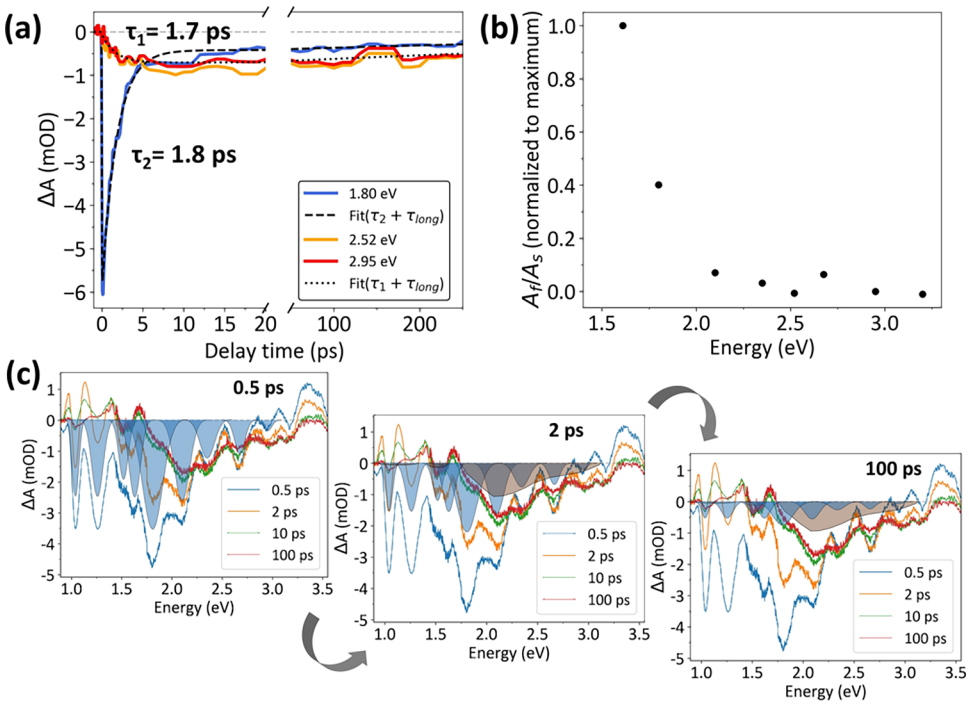

Figure 2. (a) Temporal cuts at three selected energies. The signals at 1.80 (blue line) and at 2.95 eV (red line) were fit to obtain a time constant for the fast decay (τ_2) and the delayed rise (τ_1), respectively. (b) Ratio between the weight of the faster dynamics (A_f) and the weight of slower dynamics (A_s), normalized at the maximum value, see main text, used for the fits in panel (a). (c) Qualitative sketch of the different spectral components at 0.5, 2, and 100 ps: in blue the sharp and structured peaks with fast dynamics and in brown the slow broad signal. The sketch neglects the positive signal.

difference being the signal-to-noise ratio that is worse for the thinner sample, as expected.

We now proceed to describe the PB signals in detail while, because of their low intensities, the positive contributions will be neglected. Therefore, if not otherwise specified, we will use terms like "rise time", "decay", and "peak" to refer to negative features, always meaning the module and not the sign of the signals.

The false-color map shows different rise and decay times for the various PB signals, revealing several overlapped dynamics. To show these trends, in Figure 2a, we report the temporal evolution of the PB at selected energies.

An instantaneous (shorter than the IRF (instrument response function) that is about 50 fs) appearance of a PB is observed for almost the whole energy range and is prevalent for energies below 2.30 eV. A superimposed delayed rising component (τ_1, that ends within ~10 ps) is also observed above 2.30 eV. The decay of the signals shows a fast component (τ_2, below 10 ps) that is prevalent for energies below 2.10 eV and disappears above 2.30 eV, while a slower component, τ_{long}, ≥300 ps, (our maximum time delay) has a small relative weight below 2.10 eV and is dominant above. The signals between 2.10 and 2.66 eV present a very mixed condition, in which fast and slow components have similar weights.

These features can be summarized and modeled with the overlapping of two carrier dynamics: the first one, with (slow) rise time τ_1 and (slow) decay time τ_{long}, is attributed to the presence of a broad spectral component, while the second one, characterized by instantaneous rise (within our IRF) and fast decay τ_2, is instead attributed to superimposed sharp peaks. This picture is supported by the transient map (Figure 1b) that is less structured where the slow rise dominates. It is important to notice that these two dynamics are not well-separated in energy but overlap with the weights that depend on the energy.

For this reason, we phenomenologically model the overall dynamics using the function u (see eq 1), which is the weighted sum of two functions, (fully described in the SI) representing the two dynamics. The first function (f) contains the instantaneous rise and the fast exponential decay (τ_2), observed for the sharp peaks, and prevails below 2.30 eV. The second function (g) describes the broad spectral component that shows finite exponential rise (τ_1) and slow exponential decay (τ_{long}) and prevails above 2.30 eV. To provide a visual, clarifying support to the interpretation of the spectra, we report an animated gif in Figure S3. The physical interpretation of these two components is discussed later in the text.

$$u(\tau_1, \tau_2, \tau_{long}) = A_f \cdot f(\mathrm{IRF}, \tau_2) + A_s \cdot g(\tau_1, \tau_{long}) \quad (1)$$

To evaluate the characteristic times individually and reduce the number of parameters, we fit the signal using some temporal cuts where one of the two dynamics dominates. As a typical example, the signal at 1.80 eV (shown as a blue line in Figure 2a) presents a strong instantaneous rise, a fast decay (τ_2), and a weak slow decay. Therefore, we fit this signal to evaluate τ_2 obtaining an estimation of ~1.8 ps. At 2.95 eV, on the other hand, the faster dynamics are negligible, so here, we evaluated the finite rise time (τ_1) that gives ~1.7 ps and the slow decay τ_{long} that gives ~700 ps. Another remarkable aspect of the signal is underlined by the cut at 2.52 eV, corresponding to the valley between the two peaks at 2.35 and 2.66 eV. In this case, the rise time dynamics are almost identical to that of the signal at 2.95 eV and different from the trend of the two adjacent peaks confirming the presence of two contributions to the spectra that have different characteristic times. Finally, we

https://doi.org/10.1021/acsaelm.3c00787
ACS Appl. Electron. Mater. XXXX, XXX, XXX−XXX

performed a fit for all the other peaks above 1.50 eV (see the SI for more details) that presents mixed conditions. We used the weighted sum of the two functions (f and g) fixing the three characteristic times (τ_1, τ_2, and τ_{long}) as obtained by the fits of the temporal profiles taken at three different energies and shown in Figure 2a (see eq 1).

In this fit, we used the two weighting factors (A_f and A_s) for the two functions of eq 1 as the free parameters. In order to underline the relative weight of the fast and slow components, in Figure 2b, we report the normalized ratio between A_f and A_s as a function of the various probe energies: it sharply decreases for increasing energy between 1.50 and 2.10 eV. For the sake of simplicity, in Figure 2c, the two components have been also sketched with colored areas: the fast peaks in blue and the slow bump in brown. The spectral components below 1.40 eV and above 3.10 eV are more difficult to discuss in terms of their dynamics because of the presence of overlapping positive signals that complicate the description, probably shortening their dynamics. We will not discuss the physical origin of the positive contribution to the spectra. For the physical meaning of positive signals in the FTAS spectra of semiconducting materials, we refer the reader to refs 31 and 32.

General Discussion. The overall complexity of transient absorbance signals of the Bi_2Se_3 thin film is not surprising: it has been observed in previous measurements, although only on crystalline Bi_2Se_3 films,[22,26] in a narrower energy range, limited to the visible region, with a significantly more energetic pump (above 1.4 eV) and at room temperature.[23−25,33] We primarily highlight the similarity of our data, where comparable, with those obtained on epitaxial films: this is remarkable, given the polycrystalline nature of our sample, the different growth method, and the substrate.

In contrast to our measurements, however, at room temperature, the signal mainly appears as a single, broad, and unstructured feature centered at ∼2 eV, without spectrally distinguishable peaks (we report a room temperature measurement for a pump of 2.48 eV in the SI in Figure S4). The lower energy of our pump and the low temperature allow a more accurate interpretation of the results, as we will now show.

In the literature, the PB signals are mainly discussed in terms of Pauli blocking[22,26] due to the pump-induced electron occupation of the multiple higher energy states in the band structure of Bi_2Se_3[16,17,19,30] (sketched in Figure 1). However, the pump fluences used in those works are much larger than those used here. In those papers, all the PB signals at energies below that of the pump are attributed to the direct occupation of the higher energy states involved in the corresponding transition, while any PB observed at probe energies above the pump energy was usually explained assuming a two-photon absorption of the pump. In our case, the pump energy is so small that three- to five-photon absorption should be invoked to produce features in the visible range via multiphotonic absorption, mechanisms that have cross sections that are orders of magnitude smaller than that of one-photon absorption. The linearity of the PB intensity observed in power-dependent measurements, see Figure 3, rules out any multiphoton absorption. The power dependence of the bleaching intensity does not change if a higher energy is used for the pump. The energy of the pump has no relevant effect on the shape of the spectrum either, see Figure S5 in the SI. In the absence of any nonlinear excitation, the observed PB must be explained with the depletion of occupied energy states in BVB or in SS_1, whose electrons are excited to the first BCB,

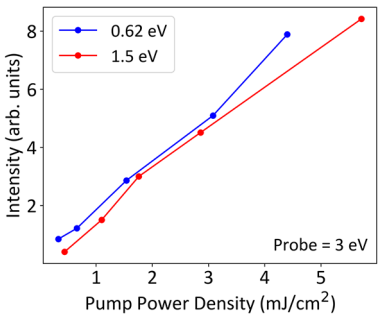

Figure 3. Intensity of the absorption bleaching as a function of the pump power density for two different pump energies, 0.62 (blue) and 1.5 eV (red).

or to SS_1 states at energy higher than E_F. In other words, all the dynamics must be described in terms of carrier relaxation and recombination only occurring in the first group of bands near the Bi_2Se_3 bandgap.

In order to reach a satisfactory model of the carrier dynamics, we only consider the contribution of the first group of bands around the bandgap and all the dynamics involving higher energy states are neglected as no electron is directly excited into those states by the pump. An important aspect that must also be considered is the presence of the two spectral components (see Figure 2c). Some useful information is found in several time- and angle-resolved photoemission spectroscopy (TR-ARPES) studies that investigated specifically the carrier dynamics occurring in Bi_2Se_3 and other similar TIs, around the bands of interest.[30,34−40] They show the presence of fast and delayed rise times and fast and slow relaxations in the same measurement. Those features are explained by an interplay of topological surface states, SS_1, and bulk valence and conduction states (BVB and BCB). An important conclusion that emerges in those works is that, given an excitation energy that only involves the first group of bands, the presence of slow, delayed responses (i.e., that last for ∼10 ps) and long relaxation times of hundreds of picoseconds, is only observed in the presence of a bulk insulator nature of the TI. Indeed, any measurement performed on bulk conductive samples only led to dynamics faster than few tens of picoseconds, with rise times below ∼1 ps. This observation presents strong analogies with our results and confirms the presence of topological states in our samples and pins the E_F between the BCB and BVB. This conclusion is also supported by previous measurements performed on our samples, grown with the same technique but on silicon, that showed E_F to be positioned in the middle of the bandgap.[12]

We conclude this first part of the discussion mentioning that a plasmon due to strongly correlated electrons has been observed at 1.026 eV using ellipsometry.[41] Therefore, it is possible that the PB observed at 1.03 eV could be given by the change of the plasmonic absorption of the probe light because of the perturbation of the electronic population provided by the pump.

A Model for the Carrier Dynamics. In Figure 4, we report a scheme depicting a qualitative description of the observed dynamics.

For $t < 0$ (i.e., before the pump excitation), the system is in equilibrium, and we have a bulk insulating TI with the BVB fully populated and the SS_1 partially populated. When the pump illuminates the sample ($t = 0$ in the left sketch of Figure 4a), some electrons are excited from states of the BVB and of

https://doi.org/10.1021/acsaelm.3c00787
ACS Appl. Electron. Mater. XXXX, XXX, XXX−XXX

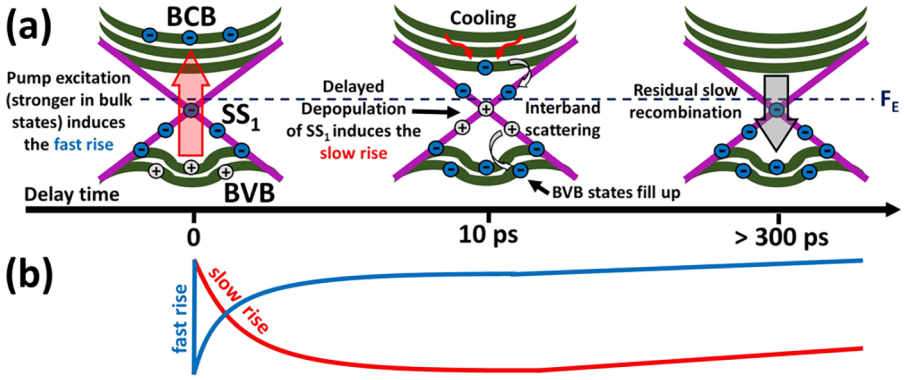

Figure 4. (a) Pictorial description of the carrier dynamics with a sequence of the carrier distribution and relaxation channels at different delay intervals. (b) Sketch of the temporal behavior of the fast and slow components. At $t < 0$ (i.e., before the pump excitation), the system is in equilibrium, and we have a bulk insulating TI with the BVB fully populated and the SS_1 partially populated. At $t = 0$ (left sketch), the red arrow indicates the excitation by the pump of the electrons from BVB to higher energy states. The direct excitation by light is responsible for the fast rise time. As discussed in the text, we suppose that SS_1 is less depopulated with respect to BVB, and for visual simplicity, in the sketch, we neglect the small instantaneous population changes occurring in SS_1 because of the excitation by the pump. Up to 10 ps, see the central sketch, carrier cooling and interband scattering occur. They are indicated by the plain red arrows and by the "black and white" arrows, respectively. The interband scattering is responsible for the slow rise (τ_1) because SS_1 states depopulate, refilling BVB. For longer times, in the sketch on the right, the gray arrow indicates the residual part of the recombination.

the SS_1 to the BCB and to higher energy states of SS_1, producing the instantaneous rise observed in the PB signals, and modeled by the IRF in the function $f(\text{IRF}, \tau_2)$ because of the depopulation of the electronic states below E_F. We expect that BVB-to-BCB transitions could be favored with respect to those SS_1-to-BCB because of the spin locking in the topological states[42,43] and by the spatially indirect character of that type of transition. This means that the SS_1 states are less depopulated than those of BVB. In the qualitative sketch of Figure 4a, we neglected any population change in SS_1 for visual simplicity.

Shortly after the excitation (up to 10 ps, see the central sketch in Figure 4a), a fast cooling of the hot carriers occurs in a few picoseconds. Contemporarily, the phonon scattering also enables interband scattering between bulk and surface states, causing carrier feeding of SS_1 from bulk carriers: this can involve both electrons (from the BCB to the upper Dirac cone of SS_1) and holes (from the BVB to the lower Dirac cone of SS_1). This process is indicated by "black and white" arrows in Figure 4a. The bulk-to-topological state scattering becomes important after the pump excitation and leads to a delayed depopulation of the lower part of the SS_1 Dirac cone, less affected by the optical excitation, producing the slow rise observed for some PB signals. This is reflected by the exponential rise with characteristic time τ_1 (present in the function $g(\tau_1, \tau_{long})$) and by the contemporary filling of the bulk states that produces the exponential decay with τ_2 in the function $f(\text{IRF}, \tau_2)$. This feature is more easily observed at high energies where a minor direct photoexcitation occurs. This kind of interband scattering was already reported by several TR-ARPES works in bulk insulating TIs[20,36,37,39,44] with similar characteristic times. Finally, as depicted in the right part of Figure 4a for $t > 10$ ps, the slow decay (τ_{long} also modeled in $g(\tau_1, \tau_{long})$) is induced by residual direct and indirect carrier relaxation. These long-living excitations, in particular the long lifetime of excited carriers in SS_1, were already observed by the previously cited works. They were explained as being due to several contributions: carrier feeding from bulk to surface states by interband scattering, a bottleneck effect at the Dirac point[37,39,45] (induced by the spin locking that prevents direct recombination through the surface states and by the reduced phase space of the Dirac point) and, primarily, a carrier separation induced by band bending near the sample surfaces, which establishes a Schottky barrier between bulk and surface states.[34,39,46] This carrier separation, in particular, strongly contributes to extending the carrier recombination time.

It is important to mention again that any TR-ARPES investigation performed on bulk conducting TI[38,39,47] shows fast dynamics, with signal lifetimes below ~10 ps. This is because the interband scattering and the band bending are reduced if E_F is pinned above the BCB or below the BVB,[38] or if in general it is too far from the Dirac point.[39] Therefore, we can consider long-lived transient absorption signals with delayed rise times as a fingerprint of the bulk insulating nature of TIs (at least in the case of a low energy pump that only excites carriers within the first group of bands).

Finally, the broad and unstructured component of the transient absorbance, which shows delayed rise and slow decay times, can be attributed primarily to the delayed depletion of the lower energy states belonging to SS_1. The large number of observed optical transitions makes it impossible to assign each of the individual spectral components of the PB signals, but their number and energy positions are compatible with the known electronic bands of Bi_2Se_3 (see Figure 1).

■ CONCLUSIONS

Making use of femtosecond transient absorption with low pump energy and at low temperatures, we have shown the presence of surface states and the bulk insulating nature of Bi_2Se_3 deposited on glass by a recently developed VSD technique. A bulk insulating nature of the material is beneficial for device operation because it gives the opportunity to better exploit its topological properties and because it allows longer-living carrier excitation. We also provided new insights into the ultrafast spectroscopic characterization of Bi_2Se_3 thanks to the low temperature and the low energy pump that allow a temporal and spectroscopic discrimination between the two main dynamics with different temporal characteristics. In particular, we have related the instantaneous signal rise with direct optical transitions and the delayed slow rise to the need

https://doi.org/10.1021/acsaelm.3c00787
ACS Appl. Electron. Mater. XXXX, XXX, XXX−XXX

for interband electronic scattering between bulk and topological electronic states to (de)populate the electronic levels involved in the bleached absorption transitions. Finally, we have clearly demonstrated that the features observed for probe energies larger than that of the pump must be interpreted without invoking multiphotonic excitation.

■ ASSOCIATED CONTENT

Supporting Information

The Supporting Information is available free of charge at https://pubs.acs.org/doi/10.1021/acsaelm.3c00787.

Vis−IR absorption spectra, further FTAS results, animations, and equations (PDF)

■ AUTHOR INFORMATION

Corresponding Author

Faustino Martelli − *Istituto per la Microelettronica e i Microsistemi−CNR (IMM-CNR), 00133 Rome, Italy;* orcid.org/0000-0002-4496-4165; Email: faustino.martelli@cnr.it

Authors

Valerio Campanari − *EuroFEL Support Laboratory (EFSL), Istituto di Struttura della Materia−CNR (ISM-CNR), 00133 Rome, Italy*

Daniele Catone − *EuroFEL Support Laboratory (EFSL), Istituto di Struttura della Materia−CNR (ISM-CNR), 00133 Rome, Italy;* orcid.org/0000-0002-7649-2756

Patrick O'Keeffe − *EuroFEL Support Laboratory (EFSL), Istituto di Struttura della Materia−CNR (ISM-CNR), 00015 Monterotondo Scalo, Italy;* orcid.org/0000-0002-8676-4436

Alessandra Paladini − *EuroFEL Support Laboratory (EFSL), Istituto di Struttura della Materia−CNR (ISM-CNR), 00015 Monterotondo Scalo, Italy;* orcid.org/0000-0002-2059-1552

Stefano Turchini − *EuroFEL Support Laboratory (EFSL), Istituto di Struttura della Materia−CNR (ISM-CNR), 00133 Rome, Italy*

Matteo Salvato − *Dipartimento di Fisica and INFN, Università di Roma "Tor Vergata", 00133 Rome, Italy;* orcid.org/0000-0002-6018-0723

Nouha Loudhaief − *Dipartimento di Fisica and INFN, Università di Roma "Tor Vergata", 00133 Rome, Italy;* orcid.org/0000-0003-3077-494X

Elena Campagna − *Dipartimento di Fisica and INFN, Università di Roma "Tor Vergata", 00133 Rome, Italy;* Present Address: Dipartimento di Scienze, Università di Roma Tre, Viale G. Marconi 446, 00146 Rome, Italy (E.C.); orcid.org/0000-0001-7121-8806

Paola Castrucci − *Dipartimento di Fisica and INFN, Università di Roma "Tor Vergata", 00133 Rome, Italy;* orcid.org/0000-0001-8986-7185

Complete contact information is available at: https://pubs.acs.org/10.1021/acsaelm.3c00787

Notes

The authors declare no competing financial interest.

■ ACKNOWLEDGMENTS

The work has been partially supported by the Project "Progetti di Gruppi di Ricerca 2020" POR FERS Lazio 2014-2020 "FOTONICS" Grant No. A0375-2020-366000. M.S. acknowledges INFN-CSN5 grant QUANTEP. P.C. acknowledges the project TESLA funded by the University of Roma Tor Vergata.

■ REFERENCES

(1) Liu, C.-X.; Qi, X.-L.; Zhang, H.; Dai, X.; Fang, Z.; Zhang, S.-C. Model Hamiltonian for Topological Insulators. *Phys. Rev. B* **2010**, *82*, No. 045122.

(2) Hasan, M. Z.; Kane, C. L. Colloquium: Topological Insulators. *Rev. Mod. Phys.* **2010**, *82*, 3045−3067.

(3) Moore, J. E. The Birth of Topological Insulators. *Nature* **2010**, *464*, 194−198.

(4) Wang, F.; Li, L.; Huang, W.; Li, L.; Jin, B.; Li, H.; Zhai, T. Submillimeter 2D Bi2Se3 Flakes toward High-Performance Infrared Photodetection at Optical Communication Wavelength. *Adv. Funct. Mater.* **2018**, *28*, 1802707.

(5) Andzane, J.; Kunakova, G.; Charpentier, S.; Hrkac, V.; Kienle, L.; Baitimirova, M.; Bauch, T.; Lombardi, F.; Erts, D. Catalyst-Free Vapour-Solid Technique for Deposition of Bi2Te3 and Bi2Se3 Nanowires/Nanobelts with Topological Insulator Properties. *Nanoscale* **2015**, *7*, 15935−15944.

(6) Zhang, H.; Liu, C. X.; Qi, X. L.; Dai, X.; Fang, Z.; Zhang, S. C. Topological Insulators in Bi 2 Se 3, Bi 2 Te 3 and Sb 2 Te 3 with a Single Dirac Cone on the Surface. *Nat. Phys.* **2009**, *5*, 438−442.

(7) Zhang, H.; Zhang, X.; Liu, C.; Lee, S. T.; Jie, J. High-Responsivity, High-Detectivity, Ultrafast Topological Insulator Bi2Se3/Silicon Heterostructure Broadband Photodetectors. *ACS Nano* **2016**, *10*, 5113−5122.

(8) Zhang, X.; Wang, J.; Zhang, S. C. Topological Insulators for High-Performance Terahertz to Infrared Applications. *Phys. Rev. B* **2010**, *82*, No. 245107.

(9) Cava, R. J.; Ji, H.; Fuccillo, M. K.; Gibson, Q. D.; Hor, Y. S. Crystal Structure and Chemistry of Topological Insulators. *J. Mater. Chem. C* **2013**, *1*, 3176−3189.

(10) He, L.; Kou, X. W. K. L.; Wang, K. L. Review of 3D Topological Insulator Thin-film Growth by Molecular Beam Epitaxy and Potential Applications. *Phys. Status Solidi RRL* **2013**, *7*, 50−63.

(11) Ginley, T. P.; Wang, Y.; Law, S. Topological Insulator Film Growth by Molecular Beam Epitaxy: A Review. *Crystals* **2016**, *6*, 154.

(12) Salvato, M.; Scagliotti, M.; De Crescenzi, M.; Castrucci, P.; De Matteis, F.; Crivellari, M.; Pelli Cresi, S.; Catone, D.; Bauch, T.; Lombardi, F. Stoichiometric Bi2Se3 Topological Insulator Ultra-Thin Films Obtained through a New Fabrication Process for Optoelectronic Applications. *Nanoscale* **2020**, *12*, 12405−12415.

(13) Orgiani, P.; Bigi, C.; Kumar Das, P.; Fujii, J.; Ciancio, R.; Gobaut, B.; Galdi, A.; Sacco, C.; Maritato, L.; Torelli, P.; Panaccione, G.; Vobornik, I.; Rossi, G. Structural and Electronic Properties of Bi2Se3 Topological Insulator Thin Films Grown by Pulsed Laser Deposition. *Appl. Phys. Lett.* **2017**, *110*, 171601.

(14) Lee, J.; Cho, D.; Chen, H.; Shim, Y. S.; Park, J.; Jeon, S. Proximity-Field Nanopatterning for High-Performance Chemical and Mechanical Sensor Applications Based on 3D Nanostructures. *Appl. Phys. Rev.* **2022**, *9*, No. 011322.

(15) Kong, D.; Randel, J. C.; Peng, H.; Cha, J. J.; Meister, S.; Lai, K.; Chen, Y.; Shen, Z. X.; Manoharan, H. C.; Cui, Y. Topological Insulator Nanowires and Nanoribbons. *Nano Lett.* **2010**, *10*, 329−333.

(16) Kim, T.; Jeong, K.; Park, B. C.; Choi, H.; Park, S. H.; Jung, S.; Park, J.; Jeong, K. H.; Kim, J. W.; Kim, J. H.; Cho, M. H. Tuning Fermi Level with Topological Phase Transition by Internal Strain in Topological Insulator Bi 2 Se 3 Thin Film. *Nanoscale* **2016**, *8*, 741−751.

(17) Wang, L.-L.; Johnson, D. D. Ternary Tetradymite Compounds as Topological Insulators. *Phys. Rev. B* **2011**, *83*, No. 241309.

(18) Soifer, H.; Gauthier, A.; Kemper, A. F.; Rotundu, C. R.; Yang, S. L.; Xiong, H.; Lu, D.; Hashimoto, M.; Kirchmann, P. S.; Sobota, J. A.; Shen, Z. X. Band-Resolved Imaging of Photocurrent in a Topological Insulator. *Phys. Rev. Lett.* **2019**, *122*, No. 167401.

(19) Tristant, D.; Vekhter, I.; Meunier, V.; Shelton, W. A. Partial Charge Transfer and Absence of Induced Magnetization in EuS(111)/Bi2Se3 Heterostructures. *Phys. Rev. B* **2021**, *104*, No. 075128.

(20) Sobota, J. A.; Yang, S.; Analytis, J. G.; Chen, Y. L.; Fisher, I. R.; Kirchmann, P. S.; Shen, Z.-X. Ultrafast Optical Excitation of a Persistent Surface-State Population in the Topological Insulator Bi 2Se 3. *Phys. Rev. Lett.* **2012**, *108*, No. 117403.

(21) Park, B. C.; Kim, T. H.; Sim, K. I.; Kang, B.; Kim, J. W.; Cho, B.; Jeong, K. H.; Cho, M. H.; Kim, J. H. Terahertz Single Conductance Quantum and Topological Phase Transitions in Topological Insulator Bi2Se3 Ultrathin Films. *Nat. Commun.* **2015**, *6*, 6552.

(22) Glinka, Y. D.; Li, J.; He, T.; Sun, X. W. Clarifying Ultrafast Carrier Dynamics in Ultrathin Films of the Topological Insulator Bi2Se3Using Transient Absorption Spectroscopy. *ACS Photonics* **2021**, *8*, 1191−1205.

(23) Glinka, Y. D.; Babakiray, S.; Holcomb, M. B.; Lederman, D. Effect of Mn Doping on Ultrafast Carrier Dynamics in Thin Films of the Topological Insulator Bi2Se3. *J. Phys.: Condens. Matter* **2016**, *28*, No. 165601.

(24) Glinka, Y. D.; Babakiray, S.; Johnson, T. A.; Bristow, A. D.; Holcomb, M. B.; Lederman, D. Ultrafast Carrier Dynamics in Thin-Films of the Topological Insulator Bi2Se3 Ultrafast Carrier Dynamics in Thin-Films of the Topological Insulator Bi 2 Se 3. *Appl. Phys. Lett.* **2015**, *103*, 151903.

(25) Kumar, N.; Ruzicka, B. A.; Butch, N. P.; Syers, P.; Kirshenbaum, K.; Paglione, J.; Zhao, H. Spatially Resolved Femtosecond Pump-Probe Study of Topological Insulator Bi2Se3. *Phys. Rev. B* **2011**, *83*, No. 235306.

(26) Jiang, T.; Miao, R.; Zhao, J.; Xu, Z.; Zhou, T.; Wei, K.; You, J.; Zheng, X.; Wang, Z.; Chen, X. Electron−Phonon Coupling in Topological Insulator Bi 2 Se 3 Thin Films with Different Substrates. *Chin. Opt. Lett.* **2019**, *17*, No. 020005.

(27) Jnawali, G.; Linser, S.; Shojaei, I. A.; Pournia, S.; Jackson, H. E.; Smith, L. M.; Need, R. F.; Wilson, S. D. Revealing Optical Transitions and Carrier Recombination Dynamics within the Bulk Band Structure of Bi2Se3. *Nano Lett.* **2018**, *18*, 5875−5884.

(28) Catone, D.; Di Mario, L.; Martelli, F.; O'Keeffe, P.; Paladini, A.; Cresi, J. S. P.; Sivan, A. K.; Tian, L.; Toschi, F.; Turchini, S. Ultrafast Optical Spectroscopy of Semiconducting and Plasmonic Nanostructures and Their Hybrids. *Nanotechnology* **2020**, *32*, No. 025703.

(29) Pelli Cresi, J. S.; Di Mario, L.; Catone, D.; Martelli, F.; Paladini, A.; Turchini, S.; D'Addato, S.; Luches, P.; O'Keeffe, P. Ultrafast Formation of Small Polarons and the Optical Gap in CeO2. *J. Phys. Chem. Lett.* **2020**, *11*, 5686−5691.

(30) Sobota, J. A.; Yang, S. L.; Leuenberger, D.; Kemper, A. F.; Analytis, J. G.; Fisher, I. R.; Kirchmann, P. S.; Devereaux, T. P.; Shen, Z. X. Ultrafast Electron Dynamics in the Topological Insulator Bi2Se3 Studied by Time-Resolved Photoemission Spectroscopy. *J. Electron Spectrosc. Relat. Phenom.* **2014**, *195*, 249−257.

(31) Pogna, E. A. A.; Marsili, M.; De Fazio, D.; Dal Conte, S.; Manzoni, C.; Sangalli, D.; Yoon, D.; Lombardo, A.; Ferrari, A. C.; Marini, A.; Cerullo, G.; Prezzi, D. Photo-Induced Bandgap Renormalization Governs the Ultrafast Response of Single-Layer MoS2. *ACS Nano* **2016**, *10*, 1182−1188.

(32) Sangalli, D.; Dal Conte, S.; Manzoni, C.; Cerullo, G.; Marini, A. Nonequilibrium Optical Properties in Semiconductors from First Principles: A Combined Theoretical and Experimental Study of Bulk Silicon. *Phys. Rev. B* **2016**, *93*, No. 195205.

(33) Kim, S.; Shin, D. H.; Kim, J. H.; Jang, C. W.; Park, J. W.; Lee, H.; Choi, S.-H.; Kim, S. H.; Yee, K.-J.; Bansal, N.; Oh, S. Resonance Effects in Thickness-Dependent Ultrafast Carrier and Phonon Dynamics of Topological Insulator Bi2Se3. *Nanotechnology* **2016**, *27*, 45705.

(34) Ciocys, S.; Morimoto, T.; Mori, R.; Gotlieb, K.; Hussain, Z.; Analytis, J. G.; Moore, J. E.; Lanzara, A. Manipulating Long-Lived Topological Surface Photovoltage in Bulk-Insulating Topological Insulators Bi2Se3 and Bi2Te3. *npj Quantum Mater.* **2020**, *5*, 16.

(35) Hajlaoui, M.; Papalazarou, E.; Mauchain, J.; Lantz, G.; Moisan, N.; Boschetto, D.; Jiang, Z.; Miotkowski, I.; Chen, Y. P.; Taleb-Ibrahimi, A.; Perfetti, L.; Marsi, M. Ultrafast Surface Carrier Dynamics in the Topological Insulator Bi 2Te 3. *Nano Lett.* **2012**, *12*, 3532−3536.

(36) Zhu, S.; Ishida, Y.; Kuroda, K.; Sumida, K.; Ye, M.; Wang, J.; Pan, H.; Taniguchi, M.; Qiao, S.; Shin, S.; Kimura, A. Ultrafast Electron Dynamics at the Dirac Node of the Topological Insulator Sb2Te3. *Sci. Rep.* **2015**, *5*, 13213.

(37) Sumida, K.; Ishida, Y.; Yoshikawa, T.; Chen, J.; Nurmamat, M.; Kokh, K. A.; Tereshchenko, O. E.; Shin, S.; Kimura, A. Inverted Dirac-Electron Population for Broadband Lasing in a Thermally Activated p-Type Topological Insulator. *Phys. Rev. B* **2019**, *99*, No. 085302.

(38) Neupane, M.; Xu, S. Y.; Ishida, Y.; Jia, S.; Fregoso, B. M.; Liu, C.; Belopolski, I.; Bian, G.; Alidoust, N.; Durakiewicz, T.; Galitski, V.; Shin, S.; Cava, R. J.; Hasan, M. Z. Gigantic Surface Lifetime of an Intrinsic Topological Insulator. *Phys. Rev. Lett.* **2015**, *115*, No. 116801.

(39) Shin, S.; Sumida, K.; Ishida, Y.; Kimura, A. *Progress in Surface Science Ultrafast Surface Dirac Fermion Dynamics of Sb 2 Te 3 -Based Topological Insulators*. 2021, *96* (2), 100628.

(40) Ciocys, S.; Morimoto, T.; Moore, J. E.; Lanzara, A. Tracking Surface Photovoltage Dipole Geometry in Bi2se3 with Time-Resolved Photoemission. *J. Stat. Mech.: Theory Exp.* **2019**, *2019*, 104008.

(41) Whitcher, T. J.; Silly, M. G.; Yang, M.; Das, P. K.; Peyrot, D.; Chi, X.; Eddrief, M.; Moon, J.; Oh, S.; Castro-Neto, A. H.; Breese, M. B. H.; Wee, A. T. S.; Silly, F.; Rusydi, A. Correlated Plasmons in the Topological Insulator Bi2Se3 Induced by Long-Range Electron Correlations. *NPG Asia Mater.* **2020**, *12*, 37.

(42) Hsieh, D.; Mahmood, F.; McIver, J. W.; Gardner, D. R.; Lee, Y. S.; Gedik, N. Selective Probing of Photoinduced Charge and Spin Dynamics in the Bulk and Surface of a Topological Insulator. *Phys. Rev. Lett.* **2011**, *107*, No. 077401.

(43) McIver, J. W.; Hsieh, D.; Steinberg, H.; Jarillo-Herrero, P.; Gedik, N. Control over Topological Insulator Photocurrents with Light Polarization. *Nat. Nanotechnol.* **2012**, *7*, 96−100.

(44) Hajlaoui, M.; Papalazarou, E.; Mauchain, J.; Perfetti, L.; Taleb-Ibrahimi, A.; Navarin, F.; Monteverde, M.; Auban-Senzier, P.; Pasquier, C. R.; Moisan, N.; Boschetto, D.; Neupane, M.; Hasan, M. Z.; Durakiewicz, T.; Jiang, Z.; Xu, Y.; Miotkowski, I.; Chen, Y. P.; Jia, S.; Ji, H. W.; Cava, R. J.; Marsi, M. Tuning a Schottky Barrier in a Photoexcited Topological Insulator with Transient Dirac Cone Electron-Hole Asymmetry. *Nat. Commun.* **2014**, *5*, 3003.

(45) Zhu, S.; Ishida, Y.; Kuroda, K.; Sumida, K.; Ye, M.; Wang, J.; Pan, H.; Taniguchi, M.; Qiao, S.; Shin, S.; Kimura, A. Supplementary Information for : Ultrafast Electron Dynamics at the Dirac Node of the Topological. *Sci. Rep.* **2015**, *5*, 13213.

(46) Yoshikawa, T.; Sumida, K.; Ishida, Y.; Chen, J.; Nurmamat, M.; Akiba, K.; Miyake, A.; Tokunaga, M.; Kokh, K. A.; Tereshchenko, O. E.; Shin, S.; Kimura, A. Bidirectional Surface Photovoltage on a Topological Insulator. *Phys. Rev. B* **2019**, *100*, No. 165311.

(47) Sánchez-Barriga, J.; Battiato, M.; Golias, E.; Varykhalov, A.; Yashina, L. V.; Kornilov, O.; Rader, O. Laser-Induced Persistent Photovoltage on the Surface of a Ternary Topological Insulator at Room Temperature. *Appl. Phys. Lett.* **2017**, *110*, 141605.

https://doi.org/10.1021/acsaelm.3c00787
ACS Appl. Electron. Mater. XXXX, XXX, XXX−XXX